Hindawi
International Journal of Aerospace Engineering
Volume 2022, Article ID 6316424, 13 pages
https://doi.org/10.1155/2022/6316424

Research Article

Experimental and Theoretical Study of Internal Pressure Loads on Boundary Walls under Gusty Wind Conditions

Sreenadh Chevula and Satya Prasad Maddula

Department of Aerospace Engineering, GITAM (Deemed to Be University), Rudraram Mandal, Sangareddy District, Patancheru, 502329 Hyderabad, India

Correspondence should be addressed to Sreenadh Chevula; ch.sreenadh@gmail.com

Received 11 March 2022; Accepted 16 June 2022; Published 12 July 2022

Academic Editor: Ratneshwar Jha

This work contains an acceptable solution to the most practical interest to reduce the internal pressure load variations acting on closed envelops (i.e., inner building walls, fairing of rocket, and missile payloads) under gusty wind conditions. To simulate the gusty wind conditions (i.e., tangential unsteady flow condition), an experimental setup of a wind tunnel with a sinusoidal gust generating mechanism has been established in IDR of the Universidad Politécnica de Madrid (IDR/UPM), Spain. The wind tunnel has been equipped with an air reservoir with vent holes. The pressure jumps shown across the vent holes are studied as a function of sinusoidal gust frequency, volume of the air reservoir, and vent hole size. A theoretical model (based on the mass conservation equation and polytropic law gas evolution) has been proposed to predict the pressure jumps and variations under gusty wind conditions. At the end of the work, theoretical and experimental results have been studied and compared. The relationship between pressure loss coefficient ξ and flow coefficient α under unsteady flow conditions has been evaluated.

1. Introduction

In general, the internal pressure of fully closed envelops or buildings depends on the position and size of accurate vent holes, the envelop adequate volume, and the external surface pressure due to the passing wind characteristics. The magnitude of internal pressure loads acting on a closed envelop or building walls is very small compared to the magnitude of external pressure loads. But a failure of walls with fully closed envelop can create a dominant opening and a vast increment in the magnitude of internal pressures. The combination of internal and large external pressure loads in the same direction causes failures in the walls of any closed envelops. Due to the obtained small magnitude of the values, the case studies of internal pressure loads have received less interest by the researchers [1]. One of the external pressure load studies, under gusty wind conditions, has been presented by Chevula et al. [2]. The first study of internal pressure loads under steady flow conditions had been introduced by Euteneuer [3]. He proposed an expression to predict the change in the internal pressure loads due to a sudden change in external pressure by neglecting the effects on the flow through the failure of envelop openings. He also found that a transient response of internal pressure may present (which causes damped oscillations too) in case of creation of a sudden opening in the closed building [1, 4]. Therefore, the failure of closed envelops or overloaded envelop components can be obtained by the vast wind flows (tropical cyclones) and huge variations in the internal and external pressure loads. The estimation of the pressure load fluctuations obtained in both steady and unsteady flow conditions on a closed building envelop is more complicated due to the complexity involved in the measurements of flow analysis parameters [5]. To overcome the complications raised, Liu and Rhee [6] presented the formulations for the internal pressure loads under steady and unsteady flow conditions. A full-scale study on internal pressure loads was conducted by Ginger et al. [7] and reported that the mean magnitude of internal pressure loads of a nominally sealed bundling or envelop is smaller than the magnitude of the external pressure loads. The internal pressure variations were measured by a model of a typical two-storey house in an open

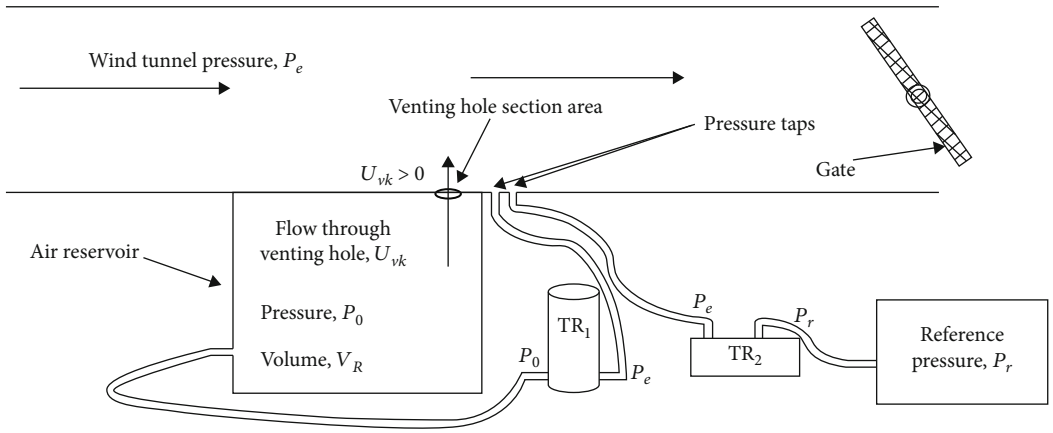

Figure 1: Schematic diagram of the experimental setup.

country exposure on various combinations of openings by Kopp et al. [8]. The internal and external pressure measurements have been obtained in the case of compartmentalizing into the connecting attic and living volumes, and the Helmholtz resonance effects have been concluded. Holmes [9] and Chaplin [10] proposed some classical methods which are relevant to calculating the influences of the internal pressures in various closed building models. In the field of space vehicle design, payload assembly, and launch, we can find some studies relevant to the internal pressure loads under gusty flow conditions, namely, space vehicle compartment vent (NASA SP-8060) [11]. Sanz-Andres et al. [12] analyzed the variation of the internal pressure loads during the climb of a spacecraft through the atmosphere. In the applications of payloads placed in fairing depressurization of spacecraft, Sanz-Andres and Navarro-Medina [13] proposed an analytical expression that can estimate the depressurization vent size.

In summary, many investigations applied linear models to obtain solutions in the study case of internal pressure loads under both steady and unsteady flow conditions. But the case study of unsteady flow conditions will result in a nonlinear formulation and solution. Along these lines, the proposed work on this paper is based on a nonlinear model analyzing the internal pressure loads under gusty wind conditions. In this paper, with the development of the nonlinear modelling of the internal pressure loads, the following assumptions are considered:

(i) Inside the reservoir (internal volume), the instantaneous pressure is uniform across the opening but changes with time (which will represent the internal pressure variations of the building in real case studies along with the time)

(ii) There is a possibility of specifying a pressure loss coefficient, ξ, to fit the theoretical and experimental data

2. Experimental Setup

The working principle of the gusty flows generating a wind tunnel and the simulation of the gusty flow conditions can be found in Chevula [2, 14] and Sanz-Andres and Navarro-Medina [13]. The experimental setup assembled with the gusty flows generating a wind tunnel can be found in Figures 1 and 2. The hardware components involved in the experimental setup can be found in Chevula [14].

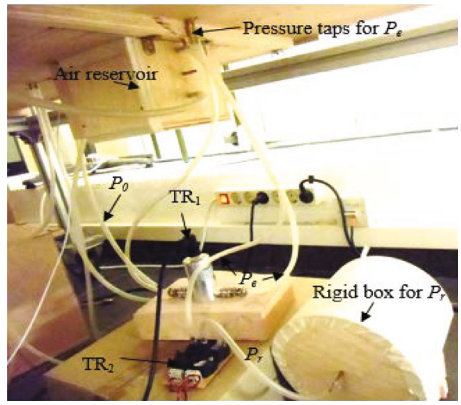

Figure 2: Experimental setup (same as Figure 1).

The flow characteristics in the test section and the frequency of the gusty flows considered for the experimental setup can be found in Chevula [2, 14, 15]. The integration of the experimental setup is based on the problem statement of the work presented in this paper, which is that a closed envelop or building is placed in a gusty flow condition. Due to the interaction between the gusty flows and the building surface (which is associated with a tangential flow around the building), a pressure field will be generated outside the building. Without any leaks from inside a closed building, the internal pressure of the building will be uniform, and a large pressure difference between the internal and external pressures of the building will appear. To reduce this significant pressure difference (or pressure jump), creating a correctly sized venting hole in the building (or envelop) can be a good solution.

Along these lines, the following steps have been initiated to create this problem statement as an experimental setup in the laboratory conditions.

(i) The flow inside the gusty wind tunnel test section is considered and modelized as the tangential

Table 1: Experimental setup.

Experimental setup parameters	Values
Reservoir's volume, V_R	0.022 m^3, 0.011 m^3, 0.0062 m^3, 0.0033 m^3, and 0.0016 m^3
Vent hole radius, R_{vh}	0.5 mm, 1.5 mm, 2.5 mm, 5 mm, 7 mm, 9 mm, 10 mm, 11 mm, and 12.5 mm
Nominal gust frequency, f_g^N	2.4 Hz, 4.0 Hz, 6.0 Hz, and 7.7 Hz
Fan rotational speed, f_m	40 Hz (i.e., U_{mv}^E = 5.5 to 6 m/s)
Length of the gate chord, L_{gc}	380 mm

unsteady flow outside the building. The closed building is viewed as a reservoir with a venting hole (see Figure 1)

(ii) An air reservoir for the reference pressure was fixed below the test section floor

(iii) The surface of the air reservoir and the floor of the test section were connected with a tube

(iv) The reference flow speed U^E inside the test section of the gusty wind tunnel was measured with a hot wire anemometer probe (1D) which was installed on the ceiling of the test section (see Figure 1)

(v) The pressure transducer TR_1 is related to the respective pressure taps Pt_1 and Pt_2 to measure the pressure jump across the vent hole ΔP (see Figure 1)

(vi) The pressure increment inside the wind tunnel, ΔP_e (see Figure 1), is measured by the pressure transducer TR_2 connected to Pt_3 and a rigid air reservoir Pr

(vii) A visible and instrumental check has been carried out to ensure no air leakage from the reservoir

3. Theoretical Model

The development of the model is based on the mass conservation equation considering the polytropic evolution inside the air reservoir [16]. A nonlinear theoretical model has been developed. Additional considerations in the development of the model are as follows:

(i) The flow exit conditions and empirical pressure loss coefficients for the flow through the vent holes are considered in the development of the model

(ii) The thermodynamic properties of the gas in the reservoir are considered homogeneous, and no spatial gradients are considered (see Holmes [1, 17]).

Because the air reservoir is made of wood which is a heat insulator and the room temperature is constant, therefore no significant temperature gradients exist:

(iii) In the venting case, the air is assumed to be a perfect gas

Table 2: Variation of $1/\sqrt{\varepsilon^E}$ as a function of the nominal gust frequency, f_g^N, vent hole radius, R_{vh}, and volume of the air reservoir, V_R.

R_{vh} (mm)	0.50	1.50	2.50	5.00	7.00	9.00	10.00	11.00	12.50
f_g^N (Hz)									
					$V_R = 0.022$ m^3				
2.4	14.8	14.8	15.2	14.7	14.4	14.8	14.2	14.8	14.5
4.0	13.3	13.2	13.3	13.2	13.2	13.2	13.2	13.1	13.3
6.0	12.0	12.0	12.0	11.8	11.8	11.9	11.9	11.9	11.8
7.7	11.2	11.4	11.4	11.3	11.3	11.3	11.3	11.3	11.3
					$V_R = 0.011$ m^3				
2.4	14.9	14.9	14.9	14.9	14.9	15.0	15.0	14.9	15.0
4.0	13.3	13.3	13.3	13.3	13.4	13.4	13.5	13.3	13.3
6.0	12.0	12.0	12.0	12.0	12.0	12.0	12.1	12.0	12.0
7.7	11.4	11.4	11.4	11.4	11.5	11.5	11.5	11.5	11.4
					$V_R = 0.0062$ m^3				
2.4	15.4	15.3	15.2	15.0	14.9	14.7	14.7	14.5	14.5
4.0	14.0	13.9	13.8	13.7	13.5	13.4	13.4	13.2	13.3
6.0	12.1	12.1	12.0	12.0	12.0	12.0	12.0	12.0	12.0
7.7	11.4	11.4	11.4	11.4	11.4	11.4	11.4	11.4	11.4
					$V_R = 0.0033$ m^3				
2.4	15.1	15.0	15.0	14.9	14.7	14.6	14.6	14.5	14.4
4.0	13.1	13.2	13.2	13.2	13.2	13.2	13.2	13.3	13.2
6.0	11.9	11.9	11.9	11.9	11.9	11.9	11.9	11.9	12.0
7.7	11.5	11.5	11.5	11.5	11.5	11.5	11.5	11.5	11.5
					$V_R = 0.0016$ m^3				
2.0	14.9	14.5	14.5	14.5	14.3	13.9	14.5	14.4	14.6
4.0	13.3	13.3	13.3	13.3	13.3	12.6	13.3	13.2	13.2
6.0	12.0	12.0	12.0	12.0	12.0	11.5	12.0	12.0	12.0
7.7	11.4	11.4	11.4	11.3	11.3	11.1	11.3	11.3	11.4

(iv) The proposed model can be applied in a closed building or envelop in which the net size of the vent is far smaller than the reference vent

From the assumption mentioned above and the homogeneous distribution of thermodynamic properties, the mass variation in the reservoir is given by

$$V_R \frac{d\rho_0}{dt} = -\rho_0 S U_{vh}, \quad (1)$$

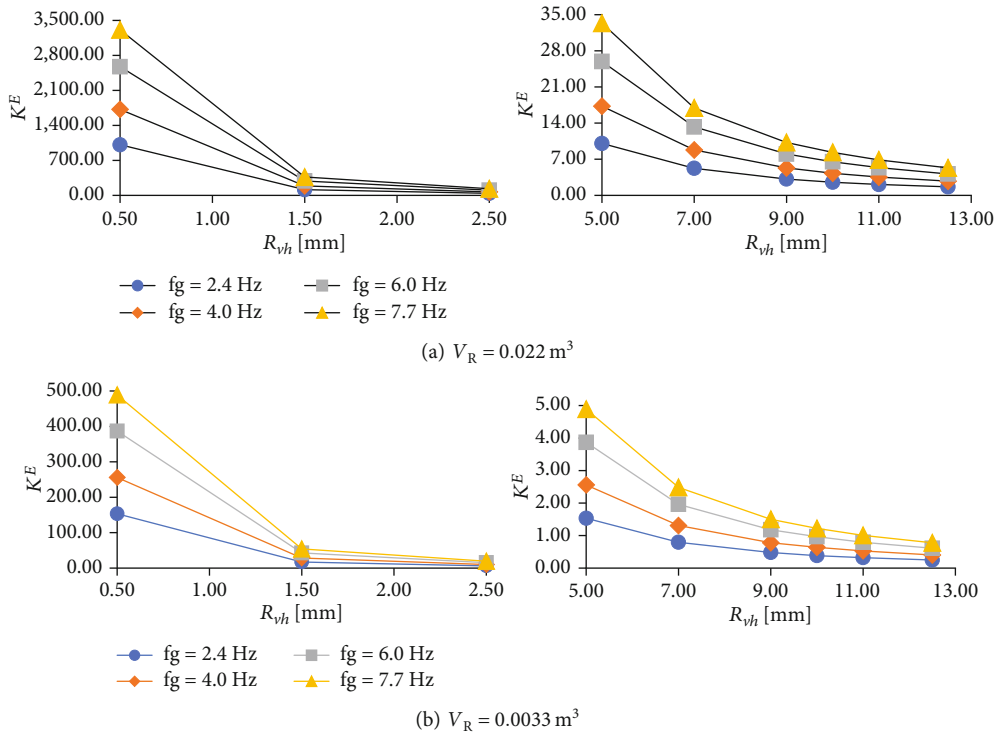

FIGURE 3: Variation of the characteristic vent time, K_E, as a function of radius of the vent holes, R_{vh}, nominal gust frequency f_g^N, and volume of the air reservoir: (a) $V_R = 0.022\ m^3$ and (b) $V_R = 0.0033\ m^3$; fan speed, $f_m = 40$ Hz (i.e., mean flow speed $U_{mv} = 5.5$ to 6 m/s).

where V_R is the reservoir volume, U_{vh} is the speed of the air flowing through the hole, ρ_0 is the density of the air in both the reservoir and the hole (considering that U_{vh} is small compared to the sound speed), and S is the section area of the vent hole. The evolution of the thermodynamic properties within the reservoir can be described by a polytropic law [16] under an isothermal process where the polytropic index n is 1.

$$\frac{P_0(t)}{\rho_0(t)^n} = \frac{P_r}{\rho_r{}^n}, \tag{2}$$

$$\rho_0(t) = \rho_r \left(\frac{P_0(t)}{P_r}\right)^{1/n}, \tag{3}$$

and, therefore,

$$\frac{d\rho_0}{dt} = \frac{\rho_r}{nP_r}\left(\frac{P_0(t)}{P_r}\right)^{(1/n)-1}\frac{dP_0}{dt}, \tag{4}$$

where the subscripts r and 0 represent initial (or reference) and instantaneous stagnation conditions in the reservoir. Concerning the flow through the vent hole, the considered case is the "where the pressure jump is small to achieve small mechanical loads on the walls." Therefore, a low speed jet is formed at the hole, and through the vent hole, incompressible flow conditions can be considered, and in fact, the assumptions are applied to equation (2). The air density in the hole is denoted as ρ_0 (no compressibility effects were included; i.e., no density changes due to speed changes are considered as the Mach number is small).

The pressure jumps across the vent hole ΔP is a consequence of the pressure loss through the vent hole:

$$\Delta P = P_0 - P_e = \frac{1}{2}\rho_0(t)U_{vh}^2\xi\ \text{sign}\ (U_{vh}), \tag{5}$$

where ξ is the total pressure loss coefficient and ΔP is measured with the pressure transducer TR_1, and $\Delta P_e = P_e - P_r \longrightarrow P_e = \Delta P_e + P_r$, where ΔP_e is the pressure difference between wind tunnel pressure, P_e, and barometric pressure P_r. ΔP_e is measured with the pressure transducer TR_2, and P_r is obtained from the lab absolute pressure transducer.

From equation (5),

$$U_{vh} = \sqrt{\frac{2|\Delta P|}{\rho_0(t)\xi}}\ \text{sign}\ (\Delta P), \tag{6}$$

and to determine the air density, the internal pressure should be known:

$$P_0 = P_e + \Delta P = P_r + (\Delta P + \Delta P_e). \tag{7}$$

Substituting equation (6) into equation (1) gives

$$\left(\frac{d\rho_0}{dt}\right)^2 = \rho_0\left(\frac{S}{V_R}\right)^2\frac{2|\Delta P|}{\xi}. \tag{8}$$

Table 3: Variation of K^E as a function of the nominal gust frequency, f_g^N, vent hole radius, R_{vh}, and volume of the air reservoir, V_R.

R_{vh} (mm)	0.50	1.50	2.50	5.00	7.00	9.00	10.00	11.00	12.50
f_g^N (Hz)									
$V_R = 0.022\,m^3$									
2.4	1013.6	113.9	41.2	10.1	5.3	3.2	2.5	2.1	1.7
4.0	1719.8	189.7	69.1	17.3	8.8	5.3	4.3	3.5	2.8
6.0	2575.1	288.1	103.9	25.9	13.3	8.0	6.5	5.4	4.2
7.7	3312.6	367.7	132.8	33.4	16.9	10.3	8.3	6.9	5.3
$V_R = 0.011\,m^3$									
2.4	517.4	57.5	20.9	5.2	2.6	1.6	1.3	1.1	0.8
4.0	848.6	94.4	34.1	8.5	4.3	2.6	2.1	1.8	1.4
6.0	1286.4	143.4	51.1	12.9	6.6	3.9	3.2	2.7	2.0
7.7	1623.7	180.8	65.3	16.2	8.3	5.0	4.1	3.4	2.6
$V_R = 0.0062\,m^3$									
2.4	295.6	32.2	11.7	3.0	1.5	0.9	0.7	0.6	0.5
4.0	478.3	53.0	19.1	4.8	2.4	1.5	1.2	1.0	0.8
6.0	722.0	80.6	29.1	7.2	3.7	2.2	1.8	1.5	1.2
7.7	910.4	101.3	36.7	9.1	4.7	2.8	2.3	1.9	1.5
$V_R = 0.0033\,m^3$									
2.4	153.4	17.3	6.2	1.5	0.8	0.5	0.4	0.3	0.3
4.0	255.7	28.5	10.1	2.6	1.3	0.8	0.6	0.5	0.4
6.0	386.9	42.7	15.3	3.9	2.0	1.2	1.0	0.8	0.6
7.7	488.8	54.1	19.5	4.9	2.5	1.5	1.2	1.0	0.8
$V_R = 0.0016\,m^3$									
2.4	76.0	8.4	3.0	0.8	0.4	0.2	0.2	0.2	0.1
4.0	122.8	13.7	5.0	1.2	0.6	0.4	0.3	0.3	0.2
6.0	187.9	20.8	7.6	1.9	1.0	0.6	0.5	0.4	0.3
7.7	238.7	26.5	9.6	2.4	1.2	0.7	0.6	0.5	0.4

Taking into account that

$$n\frac{d\rho_0}{\rho_0} = \frac{dP_0}{P_0}, d\rho_0 = \frac{\rho_0}{n}\frac{dP_0}{P_0}, \tag{9}$$

and substituting equation (9) into equation (8), one obtains

$$|\Delta P| = \left(\frac{V_R}{S}\right)^2 \frac{\xi}{2n^2}\frac{\rho_0(t)}{P_0(t)^2}\left(\frac{dP_0}{dt}\right)^2, \tag{10}$$

and from equations (6) and (1),

$$\Delta P = -|\Delta P| sign\left(\frac{dP_0}{dt}\right). \tag{11}$$

From Equation (10), it can be deduced that if the pressure jump ΔP is zero, then the derivative of the internal pressure inside the air reservoir P_0, concerning time, t, is equal to zero. At this point, the pressure jump ΔP changes its sign (then, the flow through the vent hole is reversed, and the density derivative should change sign). This behavior is also apparent in the experimental results.

In the following sections, the experimentally measured and theoretically predicted pressure differences will be distinguished by using the following notation: experimental pressure jump, ΔP^E; experimental external pressure variation, ΔP_e^E; experimental internal pressure, P_0^E; and theoretically predicted pressure jump, ΔP^T.

The theoretical pressure jump is obtained from equations (10) and (11):

$$\left|\Delta P^T\right| = \left(\frac{V_R}{S}\right)^2 \frac{\xi}{2n^2}\frac{\rho_0(t)}{P_0(t)^2}\left(\frac{dP_0^E}{dt}\right)^2, \tag{12}$$

$$\Delta P^T = -\left|\Delta P^T\right| \text{ sign}\left(\frac{dP_0{}^E}{dt}\right), \tag{13}$$

where $P_0{}^E(t)$ is obtained from equation (7). The experimental pressure jumps ΔP^E and experimental external pressure variations ΔP_e^E, measured with the pressure transducers TR_1 and TR_2, have been introduced.

3.1. Case Study: Small Pressure Jumps across the Vent Holes. The above-derived model (equation (13)) proposes to measure the pressure jumps from the venting holes, but this paper mainly focuses on where a small pressure jump across the vent holes can appear. In this line, the results obtained from the experiments (pressure jumps) with various vent hole sizes ($R_{vh} = 0.5$ mm to 12.5 mm) need to be filtered with the condition that should be fulfilled to obtain results corresponding to a small pressure jump across the vent holes. Therefore, the problem formulation in equations (2) and (8) is rewritten in dimensionless form by using as reference magnitudes the characteristic time t_c, density ρ_r, reference pressure P, and small pressure jump δ.

$$t = t_c T, \rho_0(t) = \rho\rho_r, P_0(t) = pP_r, P_e = p_e P_r, \Delta P = \delta P_r \tag{14}$$

$$\begin{aligned} p &= \frac{P_0(t)}{P_r}, \rho = \frac{\rho_0(t)}{\rho_r}, p_e = \frac{P_e}{P_r}, \\ \delta &= \frac{\Delta P}{P_r}, t_c = \frac{V_R}{Sa_r}\sqrt{\frac{\xi\gamma}{2}}, a_r = \sqrt{\frac{\gamma P_r}{\rho_r}}. \end{aligned} \tag{15}$$

In the small pressure jump depressurization range, the assumption $\delta \ll 1$ can help an asymptotic solution to be found; i.e., $\Delta P \ll P_r$ is the most frequent case ($\Delta P < 10^3$ Pa and $P_r \approx 105$ Pa).

As a first step, the variables of the problem should be expressed as power series expansion of a small parameter $\nu \ll 1$ as follows:

$$p = p_e + \nu p_1. \tag{16}$$

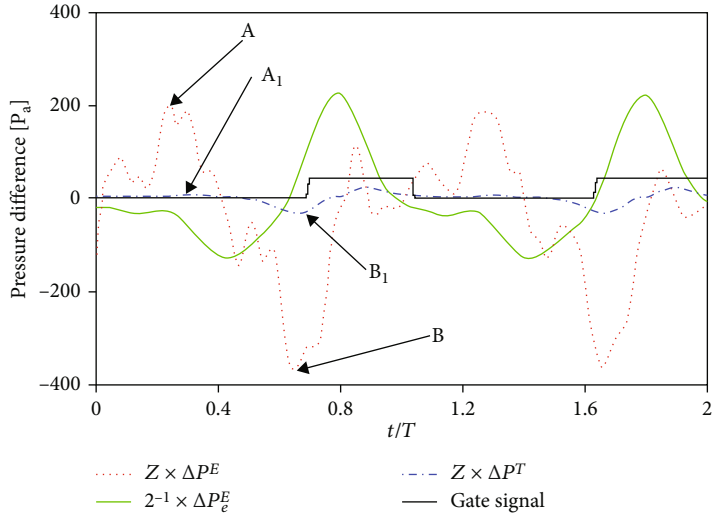

FIGURE 4: Variation of the measured pressure jump, ΔP^E, theoretical pressure jump, ΔP^T, and wind tunnel gust pressure, $\Delta P_e{}^E$, as a function of time, t, measured in the experimental setup with $f_m = 40$ Hz (i.e., $U^E_{\text{mv}} = 5$ to 6 m/s), nominal gust frequency, $f^{\text{N}}_{\text{g}} = 7.7\,Hz$, and $T = 0.129$ s. Gate signal high indicates that the rotating gate's position closes the wind tunnel duct (minimum gusty wind speed), and $R_{\text{vh}} = 12.5$ mm. $V_{\text{R}} = 0.0033\,\text{m}^3$, $Z = 10$; T is the period of a cycle; pressure loss coefficient $\xi = 1$; Z is a scale factor variable.

Substituting equation (15) into equation (16) gives

$$\frac{P_0(t)}{P_r} = \frac{P_e}{P_r} + \nu p_1 = \frac{P_e}{P_r} + \delta, \tag{17}$$

where $\delta = \nu p_1$ is the dimensionless pressure jump (i.e., the pressure load on the reservoir walls), and the density is

$$\rho_0(t) = \rho_r(p_e + \delta)^{1/n}. \tag{18}$$

Substituting equation (18) in equation (8), one obtains

$$\left(\frac{\rho_r}{nP_r}\left(\frac{P_e + \Delta P}{P_r}\right)^{(1/n)-1}\frac{d(P_e + \Delta P)}{dt}\right)^2 = \rho_0(t)\left(\frac{S}{V_{\text{R}}}\right)^2\frac{2|\Delta P|}{\xi}. \tag{19}$$

Let us assume that a sudden wind gust gives rise, g, to a pressure evolution outside the building, which is small compared to the atmospheric pressure, and then, the external pressure from equation (15) can be written as

$$P_e = P_r(1 + \varepsilon g)\,;\, \Delta P = \delta P_r\,;\, \frac{P_0(t)}{P_r} = 1 + \varepsilon g + \delta, \tag{20}$$

where

$$\varepsilon = \frac{P_e^{\max}}{P_r} - 1, \tag{21}$$

which determines the gust amplitude, $P_e^{\max}$ is the maximum value of the external pressure, and $g(t)$ is the raised dimensionless gust as a function of time. From equations (4) and (8), one obtains

$$\frac{\rho_r}{nP_r}\left(\frac{P_0(t)}{P_r}\right)^{(1/n)-1}\frac{dP_0}{dt} = -\rho_0^{1/2}\frac{S}{V_{\text{R}}}\sqrt{\frac{2|\Delta P|}{\xi}}\,\text{sign}\,(\Delta P). \tag{22}$$

Substituting equation (20) into equation (22) gives

$$\left[\frac{\rho_r}{nP_r}(1 + \varepsilon g + \delta)^{(1/n)-1}\frac{P_r d(1 + \varepsilon g + \delta)}{dt}\right]^2 = \rho_r\left(\frac{S}{V_{\text{R}}}\right)^2\frac{2|\delta|P_r}{\xi}. \tag{23}$$

In the case of large-radius vent holes, R_{vh}, the condition $\varepsilon g \gg \delta$ holds (due to the small pressure jumps across large diameter holes). Therefore, by neglecting small terms, then equation (23) leads to

$$\left[\frac{\rho_r}{n}\frac{d(\varepsilon g)}{dt}\right]^2 = \rho_r\left(\frac{S}{V_{\text{R}}}\right)^2\frac{2|\delta|P_r}{\xi}, \tag{24}$$

and thus,

$$|\delta| = \frac{1}{n^2}\left(\frac{V_{\text{R}}}{S}\right)^2\frac{\gamma\xi\rho_r}{2\gamma P_r}\left[\frac{d(\varepsilon g)}{dt}\right]^2. \tag{25}$$

From the definition (equation (15)) of the characteristic vent time, t_{c}, the first part of the left hand side can be expressed as follows:

$$t_{\text{c}}^2 = \left(\frac{V_{\text{R}}}{S}\right)^2\frac{\gamma\xi\rho_r}{2\gamma P_r} = \left(\frac{V_{\text{R}}}{Sa_r}\right)^2\frac{\xi\gamma}{2}. \tag{26}$$

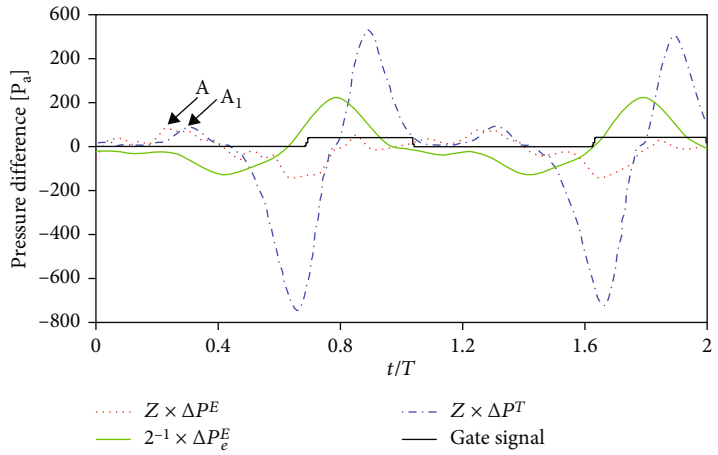

(a) Reservoir volume $V_R = 0.022\ m^3$, $Z = 1$

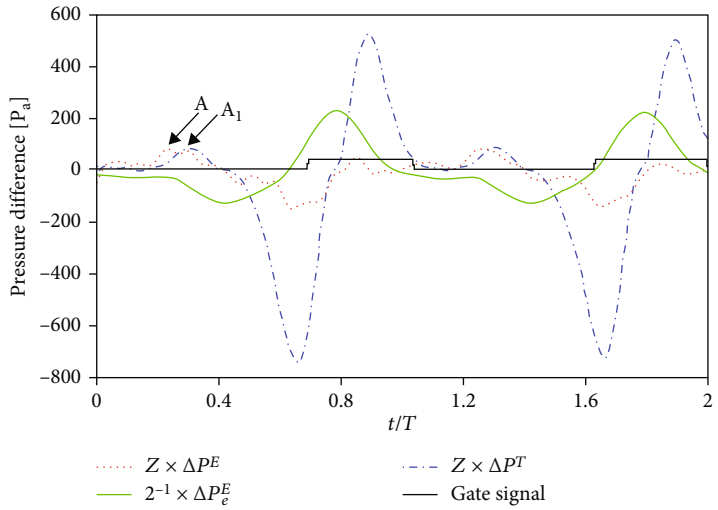

(b) Reservoir volume $V_R = 0.0033\ m^3$, $Z = 4$

FIGURE 5: Same as Figure 4, but $Z = 10$; T is the period of a cycle; positive side pressure jumps with a positive pressure loss coefficient, $\xi = \xi_{max}$.

Rewriting equation (25) by using equation (24) then gives

$$|\delta| = \frac{t_c^2}{n^2}\left[\frac{d(\varepsilon g)}{dt}\right]^2. \tag{27}$$

If the radius of the vent hole, R_{vh}, is large, then both t_c and the pressure jump δ are small (due to the small pressure jumps that arise across large-size holes).

The dimensionless gust pressure $g(t/t_g)$ is a function of Θ where $\Theta = t/t_g$ and t_g is the characteristic time of the gust evolution. Therefore, $g(t/t_g) = g(\Theta)$, and equation (27) can be written as

$$|\delta| = \frac{t_c^2}{n^2 t_g^2}\left[\frac{d(\varepsilon g)}{d\Theta}\right]^2 = \frac{K^2\varepsilon^2}{n^2}\left[\frac{d(g)}{d\Theta}\right]^2, \tag{28}$$

where $d(g)/d\Theta = O(1)$ and $K = t_c/t_g$ is the ratio of the characteristic vent time to the gust pressure variation time.

From equation (28), the order of magnitude of the δ (only in the case $\varepsilon g \gg \delta$) can be obtained:

$$|\delta| \sim K^2\varepsilon^2 \ll \varepsilon \longrightarrow K^2 \ll \frac{1}{\varepsilon} \longrightarrow K \ll \frac{1}{\sqrt{\varepsilon}}. \tag{29}$$

Equation (29) is the condition to select the experimental configurations, which gives the appropriate data to analyze the range of small pressure jumps across the vent holes. To analyze the experimental results, the dimensionless amplitude of the external pressure in experiments ε^E is defined from equation (21) as follows:

$$\varepsilon^E = \left(\frac{P_e^{\max_E} - P_r}{P_r}\right). \tag{30}$$

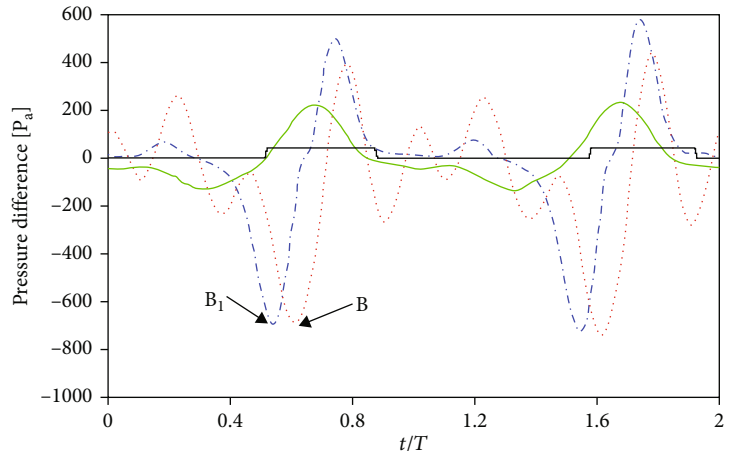

(a) $V_R = 0.022\,m^3$, $Z = 4$

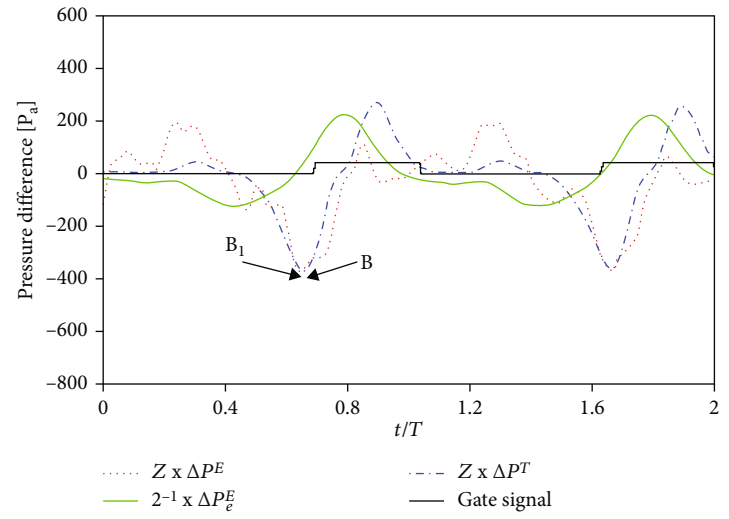

(b) $V_R = 0.0033\,m^3$, $Z = 10$

FIGURE 6: Same as Figure 4 but $Z = 10$; T is the period of a cycle; fitting the negative side pressure jumps with a negative pressure loss coefficient, $\xi = \xi_{min}$.

Considering the condition of applicability of the model for the experimental results, using equations (30) and (29), one obtains

$$K^E \ll \frac{1}{\sqrt{\varepsilon^E}}, \tag{31}$$

where superscript E represents the values taken from experiments. As a further step, the results obtained from the experimental setup (shown in Table 1) have been screened to fulfil the condition (31).

4. Experimental Results

With the obtained values from the experiments (see Table 1) and using equation (30), the minimum value of $1/\sqrt{\varepsilon^E}$ is a closer value to 11.

The data shown in Table 2 show that the influence of the reservoir volume and hole diameter is small. The pressure evaluation inside the gusty wind tunnel test section shows a drastic change due to the increased influence of the gust frequency. From the obtained experimental data, the condition (equation (31)) can be rewritten as $K^E \ll 10$ (the clear explanation of the involvements and influence of parameters t_c and t_g and required figures can be found in Chevula [14]).

From the obtained experimental data and graphical analysis (see Figure 3 and Table 3), the condition $K^E \ll 10$ is reached by the condition with vent hole $R_{vh} = 9$, 10, 11, and 12.5 mm; air reservoir volume $V_R = 0.022$, 0.011, 0.0062, 0.0033, and $0.0016\,m^3$; and nominal gust frequency $f_g^N = 2.4$, 4.0, 6.0, and 7.7 Hz. So, in this paper, the configuration mentioned above has been selected for further analysis from equation (13), and the theoretical model pressure jumps are denoted by ΔP^T. The experimental pressure

Table 4: Positive pressure jumps. Values of the total pressure loss coefficient, ξ_{max}, and flow coefficient, α_{max}, as a function of the nominal gust frequency, f_g^N, and vent hole radius $R_{vh} = 9$, 11, and 12.5 mm; reservoir volume $V_R = 0.022\,m^3$, $0.011\,m^3$, $0.0062\,m^3$, $0.0033\,m^3$, and $0.0016\,m^3$.

R_{vh} (mm)	9.00		11.00		12.50	
f_g^N (Hz)	ξ_{max}	α_{max}	ξ_{max}	α_{max}	ξ_{max}	α_{max}
			$V_R = 0.022\,m^3$			
2.4	0.5	1.36	4.8	0.46	11.4	0.30
4.0	1.2	0.90	4.6	0.47	12.0	0.29
6.0	1.4	0.84	6.4	0.40	14.3	0.26
7.7	1.6	0.78	7.3	0.37	15.2	0.26
			$V_R = 0.011\,m^3$			
2.4	6.8	0.38	27.0	0.19	33.8	0.17
4.0	7.0	0.38	28.2	0.19	55.9	0.13
6.0	7.7	0.36	29.7	0.18	58.9	0.13
7.7	11.5	0.29	35.7	0.17	66.4	0.12
			$V_R = 0.0062\,m^3$			
2.4	37.6	0.16	113.9	0.09	153.0	0.08
4.0	27.0	0.19	117.8	0.09	154.9	0.08
6.0	32.5	0.18	120.6	0.09	156.7	0.08
7.7	38.2	0.16	129.6	0.09	215.9	0.07
			$V_R = 0.0033\,m^3$			
2.4	6.2	0.40	138.4	0.08	252.8	0.06
4.0	16.4	0.25	141.2	0.08	258.8	0.06
6.0	22.2	0.21	146.5	0.08	270.7	0.06
7.7	25.5	0.20	202.6	0.07	282.3	0.06
			$V_R = 0.0016\,m^3$			
2.4	6.7	0.39	13.8	0.27	5.6	0.42
4.0	28.9	0.19	75.5	0.12	74.0	0.12
6.0	39.7	0.16	86.0	0.11	80.7	0.11
7.7	74.9	0.12	122.0	0.09	96.9	0.10

Table 5: Negative pressure jumps. Values of the total pressure loss coefficient, ξ_{min}, and flow coefficient, α_{min}, as a function of the nominal gust frequency, f_g^N, and vent hole radius $R_{vh} = 9$, 11, and 12.5 mm; reservoir volume $V_R = 0.022\,m^3$, $0.011\,m^3$, $0.0062\,m^3$, $0.0033\,m^3$, and $0.0016\,m^3$.

R_{vh} (mm)	9.00		11.00		12.50	
f_g^N (Hz)	ξ_{min}	α_{min}	ξ_{min}	α_{min}	ξ_{min}	α_{min}
			$V_R = 0.022\,m^3$			
2.4	12.9	0.24	16.5	0.24	17.2	0.24
4.0	5.0	0.35	7.1	0.35	8.0	0.35
6.0	1.9	0.50	3.4	0.50	4.1	0.50
7.7	1.4	0.51	2.7	0.51	3.8	0.51
			$V_R = 0.011\,m^3$			
2.4	29.4	0.24	38.6	0.24	51.2	0.14
4.0	12.3	0.35	15.1	0.35	23.4	0.21
6.0	6.1	0.50	8.7	0.50	15.8	0.25
7.7	5.0	0.51	8.6	0.51	12.4	0.28
			$V_R = 0.0062\,m^3$			
2.4	54.7	0.24	76.0	0.24	112.4	0.09
4.0	25.8	0.35	36.8	0.35	45.2	0.15
6.0	15.4	0.50	28.5	0.50	26.1	0.20
7.7	13.1	0.51	20.3	0.51	24.7	0.20
			$V_R = 0.0033\,m^3$			
2.4	254.4	0.24	273.9	0.24	365.5	0.05
4.0	97.4	0.35	118.2	0.35	163.9	0.08
6.0	46.5	0.50	49.7	0.50	66.1	0.12
7.7	38.2	0.51	44.0	0.51	56.7	0.13
			$V_R = 0.0016\,m^3$			
2.4	3559	0.24	7483	0.24	11131	0.01
4.0	1014	0.35	2723	0.35	10032	0.01
6.0	376	0.50	950	0.50	1319	0.03
7.7	287	0.51	639	0.51	907	0.03

jumps are denoted by ΔP^E, and measured external gust pressure is denoted by ΔP_e^E. The experimental values with the configuration of air reservoir volume $V_R = 0.022\,m^3$ and $0.0033\,m^3$ and vent hole radius $R_{vh} = 12.5$ mm are shown below.

From the plot of Figure 4, it can be observed that the obtained values of the theoretical model ΔP^T (equation (13)) and experimental pressure jump, ΔP^E, are not in agreement due to the assumed value of the pressure loss coefficient, $\xi = 1$. In a steady flow condition, the nominal value of the ξ will be in the range of 1 to 1.5 in smooth and rough surfaced vent holes [18]. But in the case of unsteady flow conditions, the value of ξ is unknown. From Figure 4, it has also been observed that the experimentally measured pressure jumps ΔP^E shows positive and negative peak values with various scale factors; i.e., the pressure loss coefficients will be different with positive and negative jumps. The same value of the pressure loss coefficient ξ will not fit both positive and negative jump directions. Various pressure loss coefficients need to be estimated for both positive and negative jump directions in this line. An empirical fitting method has been proposed to fit the maximum and minimum peak values of the positive and negative pressure jumps ΔP^T_{max} and ΔP^E_{max} and ΔP^T_{min} and ΔP^E_{min}, respectively. The empirical relationships for fitting the data are shown below.

$$\xi_{max} = \frac{\Delta P^E_{max}}{\Delta P^T_{max}} \text{ and } \xi_{min} = \frac{\Delta P^E_{min}}{\Delta P^T_{min}}, \tag{32}$$

where ξ_{max} and ξ_{min} are denoted as fitting parameters and considered the pressure loss coefficients for positive and negative pressure jumps, respectively. In Figure 4, the maximum values of positive pressure jump obtained from the experimental measurements and theoretical model are shown as A and A_1 and cannot correlate with each other. To address this problem, another theoretical positive peak value for A_1 has been chosen, which can be closer to the

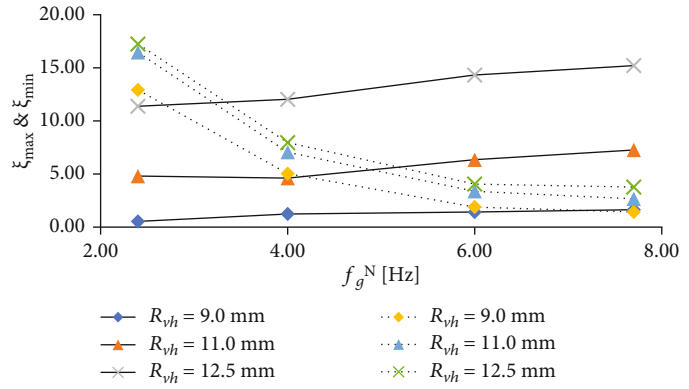

(a)

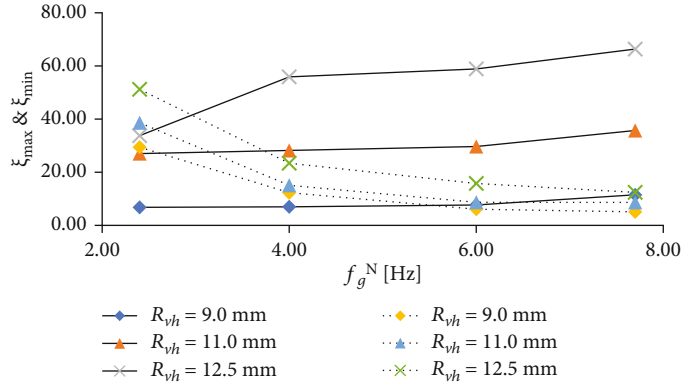

(b)

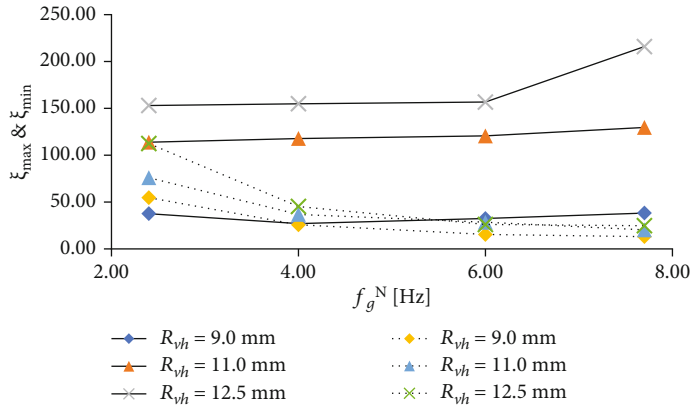

(c)

Figure 7: Continued.

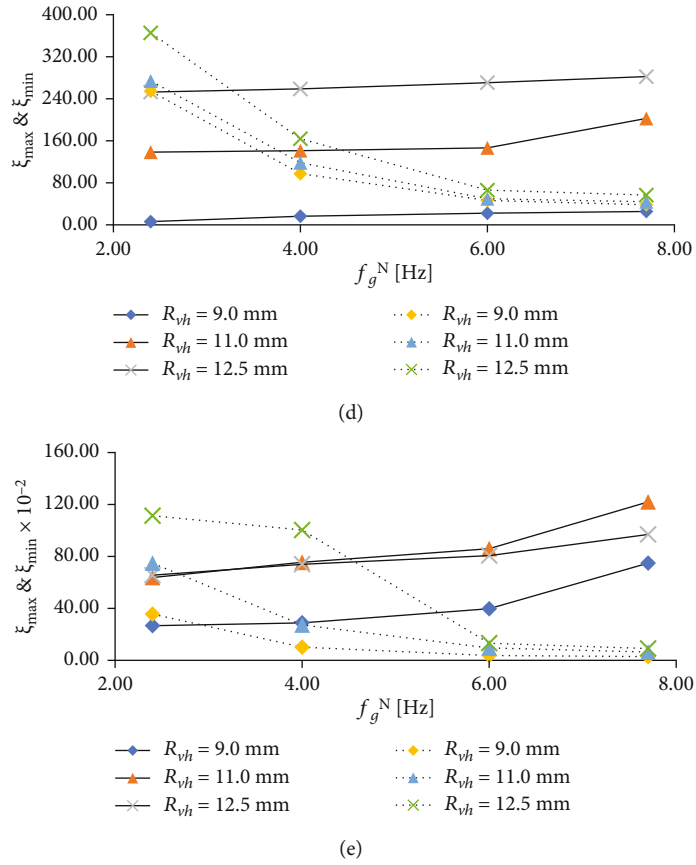

FIGURE 7: Variation of the total pressure loss coefficients, ξ_{max} and ξ_{min}, referenced to positive (solid lines) and negative (dotted lines) pressure jumps, respectively, as a function of the nominal gust frequency, f_g^N, and radius of the vent hole, R_{vh} = 9, 11, and 12.50 mm; reservoir volume V_R is (a) 0.022 m^3, (b) 0.011 m^3, (c) 0.0062 m^3, (d) 0.0033 m^3, and (e) 0.0016 m^3.

experimental peak value A and estimate the value of ξ_{max}. Similarly, in the case of negative peaks, the measured and theoretical values are shown as B and B_1, and both peaks are identified and correlated.

Figures 5 and 6 present the data with the estimated empirical values ξ_{max} and ξ_{min} and the obtained results of experimental and theoretical pressure jumps (ΔP^E and ΔP^T, respectively) and the external gust pressure ΔP_e^E.

From the data of Tables 4 and 5 and Figure 7, it can be observed that as the gust frequency increases, the obtained values from the empirical estimation of the positive and negative pressure loss coefficients, ξ_{max} and ξ_{min}, increase and decrease, respectively, which is a curious outcome from these experiments. The definition for the flow coefficient, α, and the relationship between the flow coefficient, α, and pressure loss coefficient, ξ, are presented below.

The mass flow rate through a vent hole Q_m in steady flow conditions is given by

$$Q_m = \rho_0(t) S U_{vh} = \alpha S \sqrt{2\rho_0(t)\Delta P}, \tag{33}$$

where α is the flow coefficient (denoted with the letter K in White [18]).

By substituting equation (5) into equation (33), the following relationship has been obtained:

$$\rho_0(t)^2 S^2 U_{vh}^2 = \alpha^2 S^2 \rho_0(t)^2 U_{vh}^2 \xi \tag{34}$$

is the relationship between the flow coefficient α and pressure loss coefficient ξ.

$$\alpha^2 = \frac{1}{\xi} \longrightarrow \alpha = \frac{1}{\sqrt{\xi}}. \tag{35}$$

From the empirical estimation of the pressure loss coefficients, ξ_{max} and ξ_{min}, the respective flow coefficients can also be defined from equation (33) as

$$\alpha_{max} = \frac{1}{\sqrt{\xi_{max}}}, \alpha_{min} = \frac{1}{\sqrt{\xi_{min}}}. \tag{36}$$

In the present work, to avoid confusion, the flow coefficient has been denoted by the Greek letter α, instead of the letter K denoted as the flow coefficient in the work of White [18] (in the present work, letter K is assigned to the value of a constant which relates ε and $|\delta|$ (equation (29)). The

reference data for the flow coefficient α can be found in Figure 6.41 of White [18].

Equation (36) allows us to validate the obtained experimental data in the present work with existing data in White [18], and the following points have been outlined from the same.

(i) The flow coefficient α in the literature [18] has been obtained based on the steady flow of fluid flowing from a small diameter tube 1 to another large diameter (than tube 1) tube 2

(ii) α is a function of the ratio of the diameters $\beta = d/D$, where D is the diameter of the larger tube

(iii) In the present work, the fluid flow is in unsteady condition. The positive pressure jumps relate to the flow discharge in crossflow. The negative pressure jump relates to the flow discharge inside a reservoir (with fluid at rest condition)

(iv) Unsteady flow condition is the main difference between the obtained results in this paper and White's reference literature work [18]

(v) Comparing the data of White [18] and the experimental data, the results showed that much larger room hole duct with $D = 390$ mm from White [18] and the venting hole duct with $d = 25$ mm from the experimental data of this paperwork have been obtained. The ratio of the diameters β is considered less than 0.2 in both cases (corresponding to a value of $\alpha = 0.58$ (White [18], chapter 6, Figure 6.41))

(vi) From the data of Tables 3 and 4, the extreme values obtained for the flow coefficient are $\alpha_{max} = 0.90$ and 0.10 (except the case with $V_R = 0.022$ m^3, $D_{vh} = 18$ mm and $f_g^N = 2.2\,Hz$), respectively, and for α_{min}, the obtained values are 0.84 and 0.01

(vii) The results obtained in the experiments for positive pressure jumps α_{max} are of the same order of magnitude as the flow coefficient of reference (i.e., $\alpha = 0.60$)

(viii) The results obtained in the experiments for negative pressure jumps α_{min} are also in the same range. However, the minimum value drops an order of magnitude to 0.01, in the case of small volumes of the reservoirs (i.e., $V_R = 0.0016\,m^3$)

5. Conclusions

The influence of the internal pressure variations in a closed envelop or building under gusty wind conditions has been studied. A wind tunnel with a sinusoidal gusty wind generation mechanism has been used to simulate the gusty tangential flows under various gusty wind frequencies in the test section. The experimental data have been collected across the different diameters of the venting holes D_{vh} and reservoir volumes V_R and nominal gusty frequencies f_g^N. The mean wind speed U_{mv} that has been maintained in the windburn test section is 4.5 to 5.5 m/s (approximately). A nonlinear theoretical model has been developed to predict the pressure loss coefficient ξ and flow coefficient α under unsteady flow conditions based on the gas evolution polytropic law and mass conservation equation. From the developed mathematical model, a validation condition for the experimentally obtained data $K \ll 1/\sqrt{\varepsilon}$ has been identified to filter the data. From the filtered data and observed results, it has been determined that the pressure loss coefficient ξ is not constant as in a steady flow condition. The obtained results (by fitting data) show negative and positive values for pressure loss coefficient (ξ_{min} and ξ_{max}) under unsteady flow conditions as a function of the nominal gust frequency f_g^N. After the applied values of pressure loss coefficient (ξ_{min}, ξ_{max}), the experimental and theoretical data have been in agreement with a small phase delay. Further study needs to be conducted to address phase delay, which has popped up in the agreement of results. A relationship between flow coefficient α and pressure loss coefficient ξ has been proposed to validate the obtained experimental results with the data available in the existing literature in a steady flow condition. Because of the differences in the flow condition, a good agreement between the experimental and literature data will not be expected in the validation process.

Finally, the results obtained from the conducted work conclude that the analysis of the internal pressure loads under unsteady flow conditions is a nonlinear model and will have a nonlinear solution. Linear mathematical models and solutions failed to address the solutions under unsteady flow conditions. This proposed a nonlinear mathematical model which can be a good fit for analyzing the pressure loads acting on fully closed envelops or buildings under unsteady flow conditions.

Data Availability

No data, models, or code was generated or used during the study.

Conflicts of Interest

The authors declare no conflict of interest.

References

[1] J. D. Holmes, "Mean and fluctuating internal pressures induced by wind," *Wind Engineering*, vol. 14, pp. 435–440, 1980.

[2] S. Chevula, A. Sanz-Andres, and S. Franchini, "Aerodynamic external pressure loads on a semi-circular bluff body under wind gusts," *Journal of Fluids and Structures*, vol. 54, pp. 947–957, 2015.

[3] G. A. Euteneuer, "Einfluss des Windeinfalls auf Innendruck und Zugluft erscheinung in teilweise offenen Bauwerken (influence of wind flow on internal pressure and creation of drafts in partially open buildings)," *Der Bauingenieur*, vol. 46, pp. 355–360, 1971.

[4] P. H. Liu and I. Saathoff, "Building internal pressure: sudden change," *Journal of the Engineering Mechanics Division, ASCE*, vol. 107, no. 2, pp. 309–321, 1981.

[5] B. J. Vickery, "Internal pressures and interactions with the building envelope," *Journal of Wind Engineering and Industrial Aerodynamics*, vol. 53, no. 1-2, pp. 125–144, 1994.

[6] H. Liu and K. H. Rhee, "Helmholtz oscillation in building models," *Journal of Wind Engineering and Industrial Aerodynamics*, vol. 24, no. 2, pp. 95–115, 1986.

[7] J. D. Ginger, K. C. Mehta, and B. B. Yeatts, "Internal pressures in a low-rise full-scale building," *Journal of Wind Engineering and Industrial Aerodynamics*, vol. 72, pp. 163–174, 1997.

[8] G. A. Kopp, J. H. Oh, and D. R. Inculet, "Wind-induced internal pressures in houses," *Journal of Structural Engineering, ASCE*, vol. 134, no. 7, pp. 1129–1138, 2008.

[9] J. D. Holmes, *Wind Loading of Structures; Spon Press Publications: London*, CRC Press, Florida, 2001.

[10] G. Chaplin, *Turbulent Wind Interactions with Ventilated Structures, [Ph.D. thesis]*, University of Nottingham, Nottingham, UK, 1997.

[11] NASA SP-8060, *NASA Space Vehicle Design Criteria Compartment Vent*, National Aeronautics and Space Administration, Washington, DC, USA, 1970.

[12] A. Sanz-Andres, J. Santiago-Prowald, and A. Ayuso-Barea, "Spacecraft launch depressurization loads," *Journal of Spacecraft and Rockets*, vol. 34, no. 6, pp. 805–810, 1997.

[13] A. Sanz-Andres and F. Navarro-Medina, "The initiation of rotational motion of a lying object caused by wind gusts," *Journal of Wind Engineering and Industrial Aerodynamics*, vol. 98, no. 12, pp. 772–783, 2010.

[14] S. Chevula, *Aerodynamic Loads Acting on Bluff Bodies under Wind Gusts, [Ph.D. thesis]*, UPM, Madrid, Spain, 2015.

[15] S. Chevula, Á. Sanz-Andres, and S. Franchini, "Estimation of the correction term of pitot tube measurements in unsteady (gusty) flows," *Flow Measurement and Instrumentation*, vol. 46, pp. 179–188, 2016.

[16] J. Christians, "Approach for teaching polytropic processes based on the energy transfer ratio," *International Journal of Mechanical Engineering Education*, vol. 40, no. 1, pp. 53–65, 2012.

[17] R. N. Sharma and P. J. Richards, "Discussion of net pressures on the roof of a low-rise building with wall openings," *Journal of Wind Engineering and Industrial Aerodynamics*, vol. 93, no. 4, pp. 267–291, 2005.

[18] M. F. White, *Fluid Mechanics*, McGraw-Hill, New York, NY, USA, 2011.